iScience

CellPress
OPEN ACCESS

Article

# Theoretical investigation on the effect of terahertz wave on $Ca^{2+}$ transport in the calcium channel

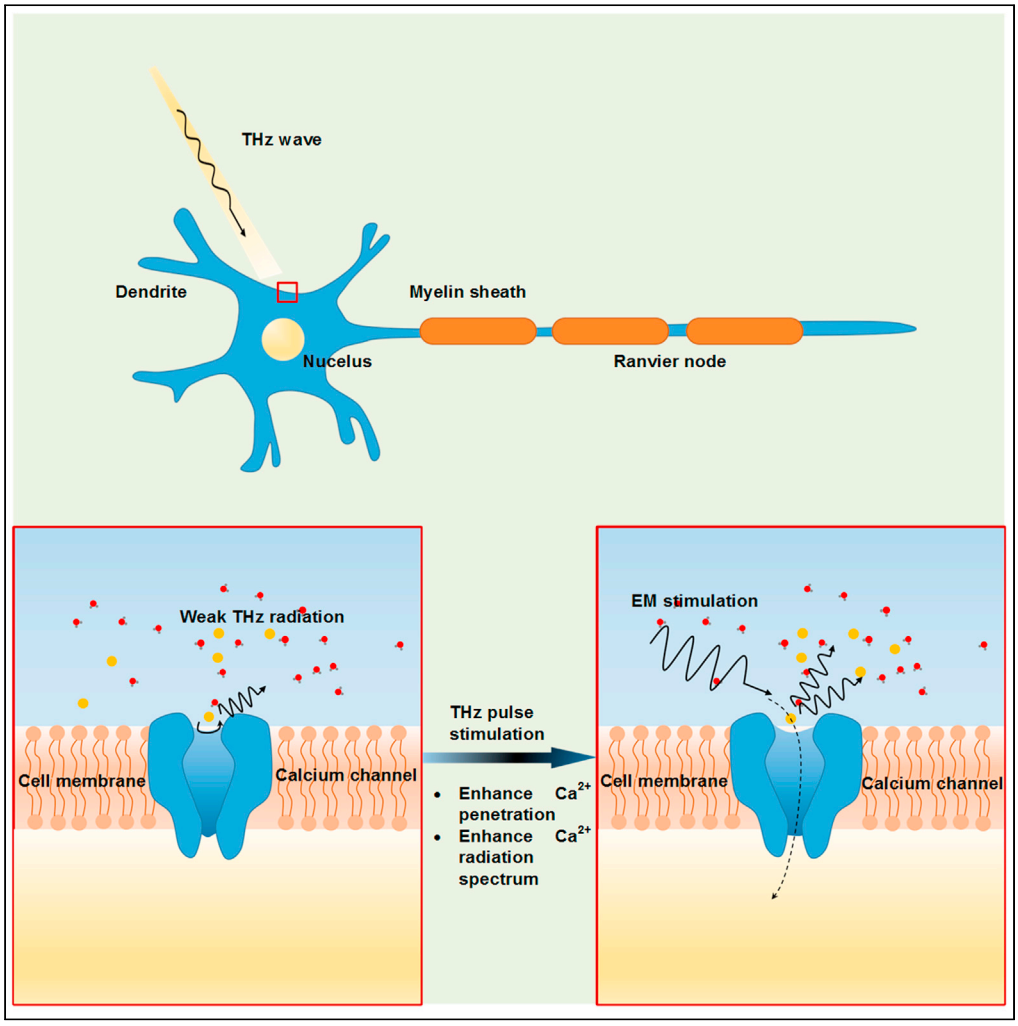


Lianghao Guo, Wenfei Bo, Kaicheng Wang, Shaomeng Wang, Yubin Gong

wangsm@uestc.edu.cn (S.W.)
ybgong@uestc.edu.cn (Y.G.)

## Highlights

We demonstrate the THz radiation generated by $Ca^{2+}$ transport in the channel

External THz stimulation can enhance the radiation spectrum of $Ca^{2+}$

External THz stimulation can accelerate the transport of $Ca^{2+}$ across the membrane

Guo et al., iScience 25, 103561
January 21, 2022 
https://doi.org/10.1016/j.isci.2021.103561

iScience

CellPress
OPEN ACCESS

Article

# Theoretical investigation on the effect of terahertz wave on $Ca^{2+}$ transport in the calcium channel

Lianghao Guo,[1] Wenfei Bo,[3] Kaicheng Wang,[1] Shaomeng Wang,[1,2,*] and Yubin Gong[1,2,4,*]

## SUMMARY

**The question of whether terahertz (THz) waves can interact with ions in channels of nerve cells and cause a further reaction has attracted much attention. To answer this question, we investigate the spontaneous radiation generated by $Ca^{2+}$ moving in calcium channels and the effect of THz radiation on the transport of $Ca^{2+}$ by solving the mathematical physical model through Brownian dynamics (BD) simulations. It is obtained that the moving $Ca^{2+}$ in a calcium channel can generate electromagnetic radiation, the corresponding spectrum of which is concentrated in the THz range. Meanwhile, both the ion number in the channel and the background temperature are proved to have significant effects on the spontaneous emission spectra. The studies also show that external THz radiation can accelerate $Ca^{2+}$ transport through the ion channel. These results are expected to provide a theoretical basis for the future treatment of THz waves in the neurological field.**

## INTRODUCTION

$Ca^{2+}$ and Calcium channels play important roles in many physiological and biological functions, from heart contraction to gene transcription, and from signaling in the nervous system to triggering muscle contractions. Therefore, it is important to understand the precise feedback mechanisms that allow calcium ions to enter cells.

It has been reported that in addition to traditional electrical stimulation, light stimulation (Kato et al., 2012), sound stimulation (Ibsen et al., 2015), pain stimulation (Caterina et al., 1997), and pressure stimulation (Ranade et al., 2015) can promote ion transport across the membrane. However, there are few reports on ion transport stimulated by high-frequency electromagnetic stimulation. THz wave, as a kind of electromagnetic wave with low electronic energy level and high temporal and spatial resolution, has been widely used in electromagnetic biology research at the cellular and even molecular level in recent years. The biophotons produced by various intracellular oxidative metabolism processes happen to be in the THz band (Miller and Dumas, 2010; Wetzel and LeVine, 1999), proving that organisms have a wealth of THz information. Thus, THz waves have various potential applications in biological physics: they can be used to analyze the fingerprint spectrum of biological materials, stimulate proton transfer in base-pair hydrogen bonds (Wang et al., 2020), and accelerate DNA molecular unwinding (Wu et al., 2020).

THz waves have also been proved to have great potential for application in the field of neural research. It was claimed that through experiments and simulations verification, nerve fibers can be regarded as dielectric waveguides transmitting THz and mid-infrared waves (Kumar et al., 2016; Liu et al., 2019; Zangari et al., 2018). Studies showed that THz waves can regulate neural activity, and can enhance the permeability of the Voltage-Gated Calcium Channel (VGCC) by influencing the corresponding chemical bonds of —$COO^-$ or —C=O(Li et al., 2021).

Based on available scientific reports, we need to think about whether high-frequency electromagnetic radiation will be generated during the oscillation and transport of ions in the channels, and whether the spontaneous radiation will be affected by external stimulus? Therefore, this paper uses Calcium ion channels as a research object to investigate the spontaneous radiation of ions moving in channels. The schematic diagram of the basic model is shown in Figure 1. The main contents of this paper are as follows: (1) based on

[1]School of Electronic Science and Engineering, University of Electronic Science and Technology of China, Chengdu, Sichuan 610054, China

[2]National Key Lab on Vacuum Electronics, Medico-Engineering Cooperation on Applied Medicine Research Center, School of Electronic Science and Engineering, University of Electronic Science and Technology of China, Chengdu, Sichuan 610054, China

[3]National University of Defense Technology, Xi'an, Shaanxi 710106, China

[4]Lead contact

*Correspondence: wangsm@uestc.edu.cn (S.W.), ybgong@uestc.edu.cn (Y.G.)

https://doi.org/10.1016/j.isci.2021.103561

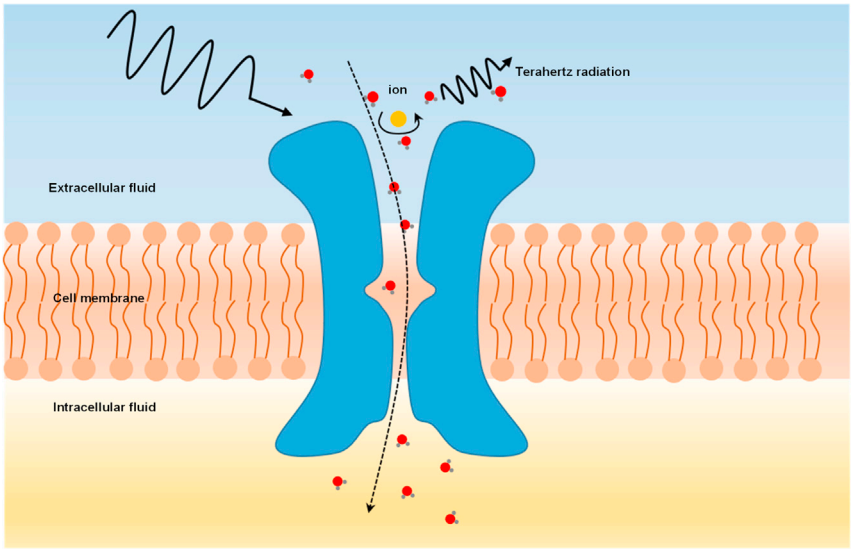


**Figure 1. Schematic diagram of THz waves regulating calcium ion transport across membranes and ions producing THz radiation**

previous studies on BD simulation of the ion channel(Corry et al., 2001; Hoyles et al., 1998; Li et al., 1998), the three-dimensional potential energy distribution of the calcium channel is obtained in this paper to study the electromagnetic radiation generated during the transport of calcium ions across the membrane, aiming to explain the conjecture proposed in the ref (Liu, 2018), which is "the existence of high-frequency electromagnetic signals from THz to infrared in the biological nervous system; (2) we investigate the influence of temperature and the number of $Ca^{2+}$ on the THz radiation generated by the moving $Ca^{2+}$ in the channel; (3) we study the regulation of the external THz field on the movement of single ion and multiple ions, aiming to reveal the preliminary theoretical demonstration of the influence of the THz field on the production and conduction of neural action potentials. Studying the effect of THz waves on the ion penetration in $Ca^{2+}$ channels can provide an approach not only for correcting an abnormal $Ca^{2+}$ conduction process for normal cells but also for inducing rapid apoptosis of unwanted cells like malignant tumors by increasing $Ca^{2+}$ flow to overload calcium concentration(Orrenius et al., 2003).

## RESULTS AND DISCUSSION

### Geometric properties of calcium ion channel

It is well known that the $Ca^{2+}$ channel mainly consists of a central water channel, which narrows from the central water area to both sides and connects the inner and outer cell sap of the cell membrane (Corry et al., 2001; McCleskey and Almers, 1985). The highly charged glutamate residues are distributed on the channel proteins connecting to a segment of the membrane, forming a negatively charged ring, which acts as a selective filter for ion transmembrane transports.

The calcium channel model used in this paper is constructed based on the model in the Ref (Corry et al., 2001). The two-dimensional (2D) model of the $Ca^{2+}$ channel is shown in Figure 2, where the diamonds represent glutamate residues, and the triangles represent the dipoles. The three-dimensional (3D) model can be obtained by rotating the 2D model 180° along the axis $r = 0$, so that there are four dipoles and glutamate residues distributed on either end of the 3D channel, respectively. The charge of each dipole is $0.6 \times 10^{-19}$C, with the length of 5 Å at $z = -17.5$ Å. These dipoles are used to represent the charged side chains thought to form a ring around the entrance of the constricted region and their nearby counter-charges. It is noteworthy that the glutamate residues are distributed asymmetrically on the boundary of the neck area of the channel (Bahinski et al., 1997; Ellinor et al., 1995), which is used to simulate selective filtration. The four charges are placed at $z = 10.5$ Å, 11.83 Å, 13.17 Å, and 14.5 Å with adjacent angular distances of 90°. The glutamate residues are with the same charge of $-1.3 \times 10^{-19}$C for each and are placed on the inner wall of the channel with a distance of 1 Å from the boundary. The values of the charges in the model are obtained from Ref (Corry et al., 2001).

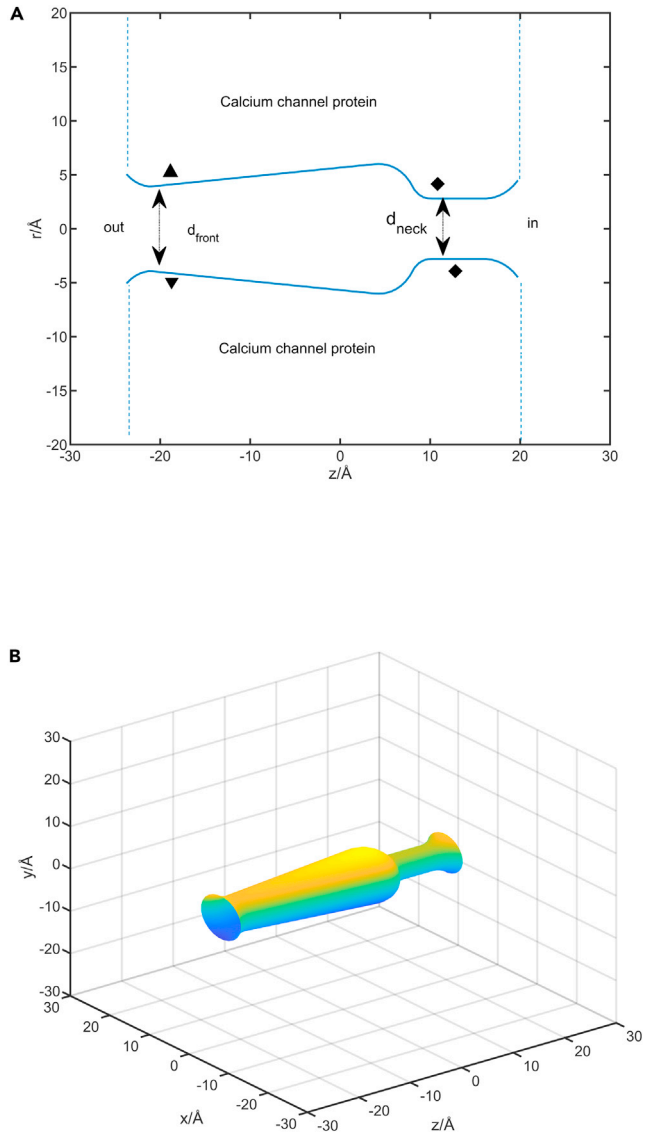


**Figure 2. The physical model of calcium channel**

(A) The 2-D model of the calcium channel, where ▲ represents the dipoles and ◆ represent the glutamic charges.
(B) The 3-D model of the calcium channel is obtained by the rotation of figure (A) by 180° along the axis.

The ion-channel interaction includes two components: a repulsive force because of the induced charges on the protein boundary and an attractive force because of the electrostatic interaction of the ion with charge residues and dipoles on the channel wall. The induced charges on the protein boundary are related to the ions' positions in the channel. To describe the relationship between the induced charge and the ion, we located the $Ca^{2+}$ at an initial position (0, 0, -4 nm) firstly and calculated its induced charge on the protein wall. Then move the ions forward in steps of 1Å and calculate the induced charge on the wall of the channel protein at the next position. Because solving the Poisson equation at every time step will greatly increase computation, the look-up table method (Hoyles et al., 1998) is used in this paper to store the pre-calculated electric fields and potential values of ions at all positions in the channel.

The relationship between ions with the induced charge on the water-protein boundary is shown in Figure 3, and the calculation method is shown in the method details section. The induced surface charge increases as the $Ca^{2+}$ comes close to the channel neck area. Meanwhile, the induced surface charge shows the same electrical properties as $Ca^{2+}$, which will give the $Ca^{2+}$ a repulsive force when it gets close to the boundary.

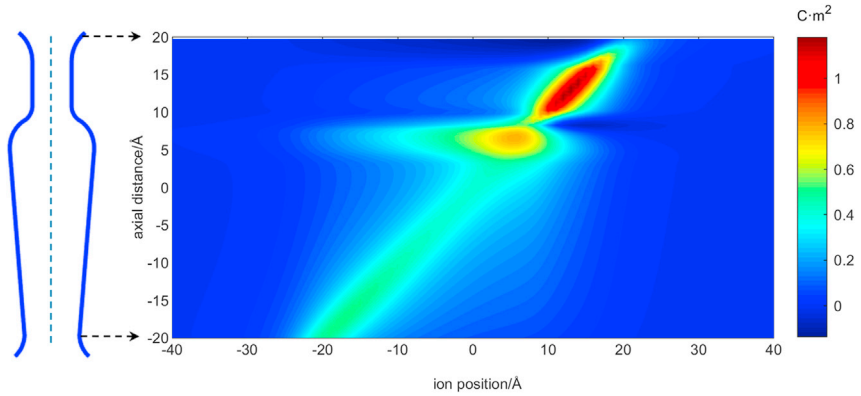


**Figure 3. Polarization charge density on the channel wall**

The x axis represents the position of the ions along the axis, the y axis represents the axial distance. The induced surface charge increases as the $Ca^{2+}$ comes close to the channel neck area. Meanwhile, the induced surface charge shows the same electrical properties as $Ca^{2+}$, which will give the $Ca^{2+}$ a repulsive force when it gets close to the boundary.

## Potential energy distribution

The force on ions in the channel mainly includes three parts: the repulsive force from the induced charge at the channel boundary, the attraction force from the negatively charged groups of the channel, and the Coulomb force among the ions. For single $Ca^{2+}$, the potential energy profile is constructed by calculating the movement of ions from infinity to a fixed position. Repeating this process can obtain the channel potential energy diagram. The dielectric constant of water inside the VGCC channel is different from free water ($\varepsilon = 78$). Especially in the neck areas, because of the negatively charged groups, the dielectric constant

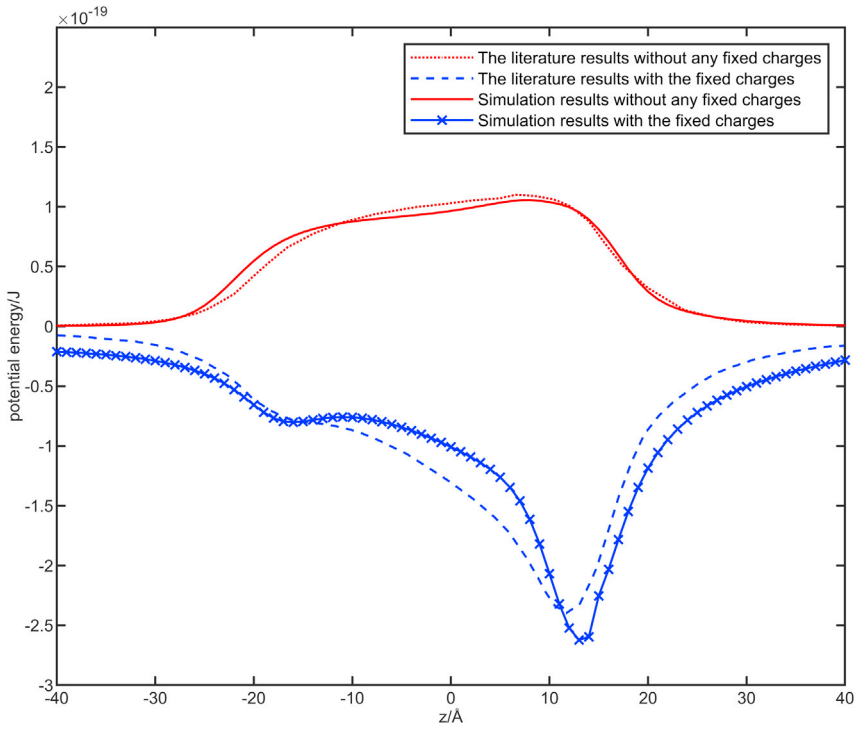


**Figure 4. Comparison of simulation results and reference results**

The solid red line is the potential energy curve on the channel axis without considering the fixed charge on the boundary, whereas the dotted red line is the calculation result in the corresponding literature; the solid blue line is the curve of potential energy on the axis of the channel when the interaction of negatively charged groups is considered, and the dashed blue line is the calculation result in the corresponding literature.

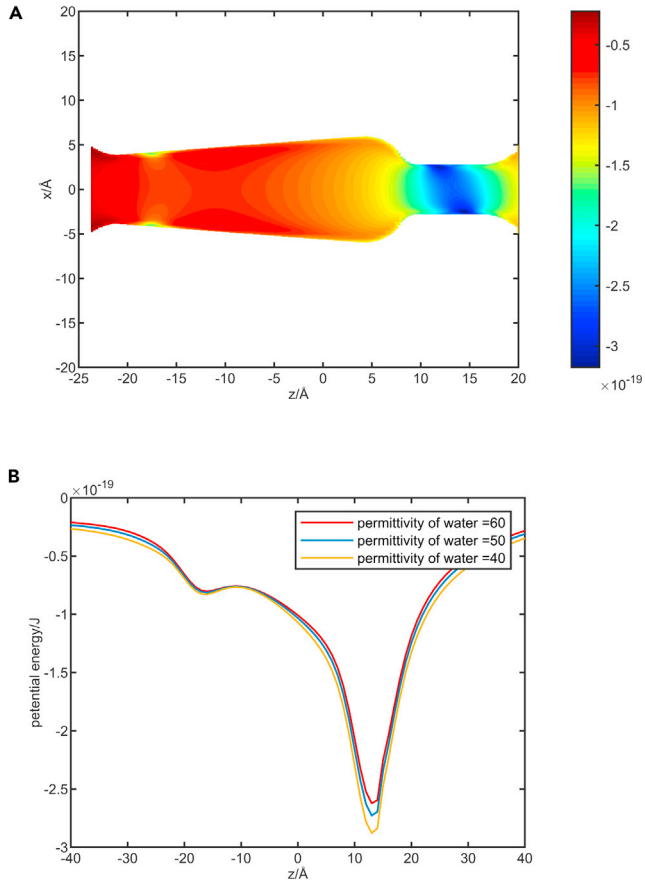


**Figure 5. Potential energy distribution in the calcium channel**

(A) The 2-D potential energy diagram of the calcium channel.

(B) The potential energy curve of the channel axis with different dielectric constants of water.

of water is significantly lower than that of the vestibule and free water. As a compromise, the same dielectric constant of water ($\varepsilon = 60$) is used in the pores and the reservoirs. The calculation method of potential energy is shown in the method details section. To verify the correctness of the model, the results are compared with it in ref (Corry et al., 2001) as shown in Figure 4.

$Ca^{2+}$ entering the channel from outside of the membrane will be constrained by the attraction force of the negatively charged ring near the lowest point of potential energy and will meet a steeply rising potential barrier that is proportional to the square of the $Ca^{2+}$ charge before the exit. Figure 5A shows the potential energy diagram of the 2D potential energy along the section $y = 0$. The lowest potential energy appears near the channel neck and shows increasing trends from the central axis to both sides.

$Ca^{2+}$ transport across the membrane in the form of hydration, but $Ca^{2+}$ and charged residues at the channel boundary will generate strong local electric fields, making the polarization degree of water inside the channel significantly different from that of free water. The degree of polarization of water can be characterized by the dielectric constant. As water plays an important role in the $Ca^{2+}$ transport crossing the channel, we calculate the influence of the dielectric constant of channel water on the barrier height. It is worth noting that the height of the channel barrier varies with the dielectric constant of channel water. Figure 5B shows the potential energy curve on the central axis varies with the permittivity of water. When the permittivity of channel water was chosen to be as 60, 50, and 40, the height of the barrier increased accordingly.

The quantitative relationship between barrier height and the permittivity of channel water is shown in Figure 6. The results show that as the dielectric constant of the channel water decreases, the barrier height

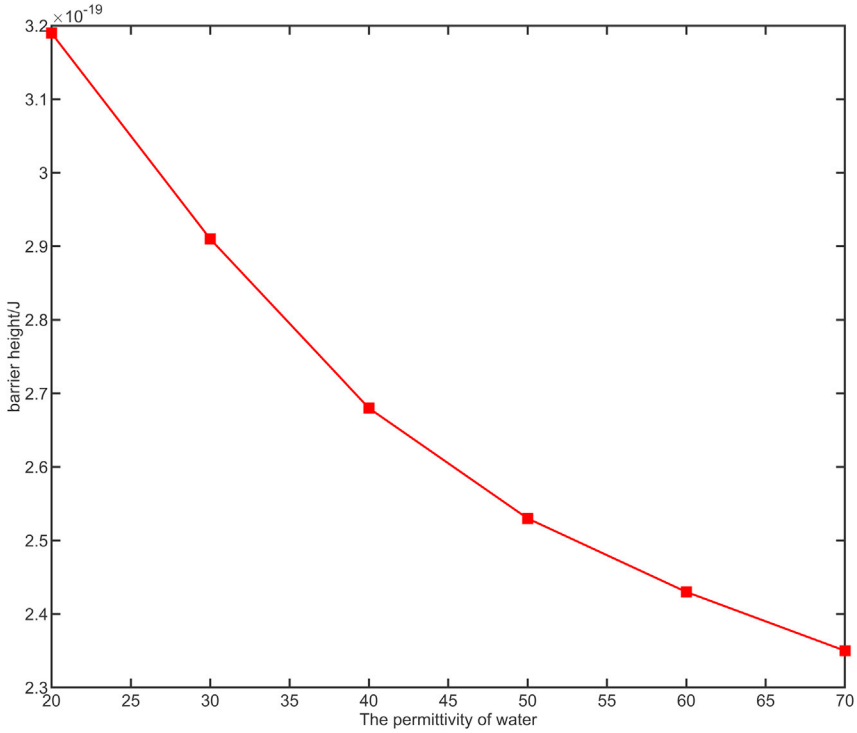


**Figure 6. The relation between the height of the channel barrier and the dielectric constant of the channel water**
As the dielectric constant of the water inside the channel decreases, the barrier to overcome for $Ca^{2+}$ to pass through the channel increases significantly.

increases significantly. Here, we make a compromise and set the dielectric constant of the water inside the channel to 60 to complete the following calculation.

## Ion motion and spontaneous radiation analysis

In the simulation to obtain the dynamic equilibrium of $Ca^{2+}$ inside of the channel, the initial configuration of the $Ca^{2+}$ is randomly distributed in the simulation region by generating a stochastic number. Without an external electric field, the $Ca^{2+}$ in the simulation area will be attracted by the negatively charged ring in the neck area of the channel and move to the lowest point of potential energy near 1.25Å and move randomly. By solving Equations (10) and (11), the positions and velocities of the ion at different times can be obtained, as shown in Figure 7. The parameters used during the calculation progress are listed in Table 1.

Here, the spontaneous radiation spectrum of $Ca^{2+}$ movement can be obtained by applying the Fourier transform of the electric field generated by calcium ion movement. The electric field emitted by ion motion can be obtained by Equation (1) (Jackson, 1999),

$$\vec{E}_{rad} = \frac{q}{c^2}\frac{1}{d}[\hat{n} \times (\hat{n} \times \hat{a})]_{ret} \qquad \text{(Equation 1)}$$

where $q$ is the charge of $Ca^{2+}$, $d$ is the distance between the measurement point and the ion, $c$ is the speed of light, $\hat{n}$ is the unit vector of the electric charge pointing in the direction of the observation point, and $\hat{a}$ is the accelerated speed, which can be obtained by taking the derivative of Equation (11). The total radiation spectrum can be obtained from the radiation spectrum in the three directions. The results are shown in Figure 8. As can be seen, the spectrum of calcium ions moving in the channel is mainly concentrated around 16.9THz.

The process of ion transport is the continuous movement of ion current from one side of the membrane to the other. Based on the analysis of the motion of a single ion, we studied the changes in the spontaneous

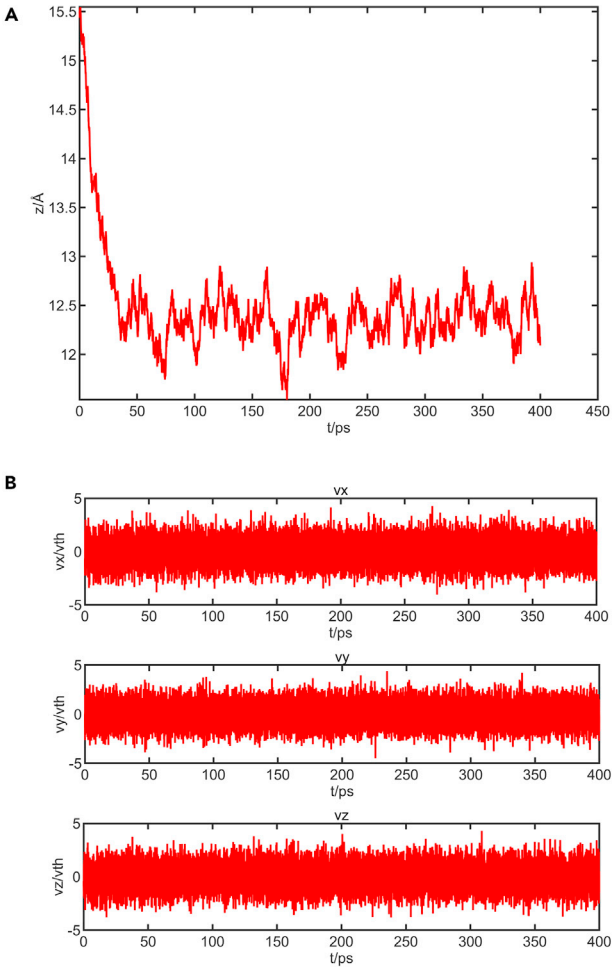


**Figure 7. The relationship between the position and velocity of the ion changes with time without external stimulus**

(A) The axial position of single $Ca^{2+}$. It will be constrained to do random movement near the lowest point of potential energy (z = 12.5Å) without external stimulus.

(B) The ion velocity varies with time in the directions of x, y, z.

**Table 1. The relevant parameters of the Brownian dynamic method used to calculate $Ca^{2+}$ motion**

| Parameters | Description | Value |
|---|---|---|
| $m_i$ | $Ca^{2+}$ mass | $6.6 \times 10^{-26}$kg |
| $Q$ | $Ca^{2+}$ charge | $3.2 \times 10^{-19}$C |
| $Di$ (Corry et al., 2001) | $Ca^{2+}$ diffusion coefficient | $0.79 \times 10^{-9}m^2/s$ |
| $K_B$ | Boltzmann constant | $1.38 \times 10^{-23}$J/K |
| $T$ | Temperature | 310K |
| $R_i$ | $Ca^{2+}$ radius | 0.99 Å |
| $F_0$ (Stillinger and Rahman, 1974) | the force field parameter | $2 \times 10^{-10}$N |
| $R_B$ (Tansel et al., 2006) | $Ca^{2+}$ hydration radius | 2.6 Å |
| $R_w$ (Stillinger and Rahman, 1974) | the radius of boundary wall atoms | 1.4 Å |
| $C_0$ (Corry et al., 2001; Guàrdia and Padró, 1996; Guàrdia et al., 1993) | Coefficient $C_0$ for $Ca^{2+}$-$Ca^{2+}$ pair | 0.8 $K_BT$ |
| $C_1$ (Corry et al., 2001; Guàrdia and Padró, 1996; Guàrdia et al., 1993) | Coefficient $C_1$ for $Ca^{2+}$-$Ca^{2+}$ pair | 1.6 Å |
| $C_2$ (Corry et al., 2001; Guàrdia and Padró, 1996; Guàrdia et al., 1993) | Coefficient $C_2$ for $Ca^{2+}$-$Ca^{2+}$ pair | 1.8 Å |
| $C_3$ (Corry et al., 2001; Guàrdia and Padró, 1996; Guàrdia et al., 1993) | Coefficient $C_3$ for $Ca^{2+}$-$Ca^{2+}$ pair | 1 Å |
| $c_w$ (Corry et al., 2001; Guàrdia and Padró, 1996; Guàrdia et al., 1993) | Coefficient $c_w$ for $Ca^{2+}$-$Ca^{2+}$ pair | 2.76 Å |

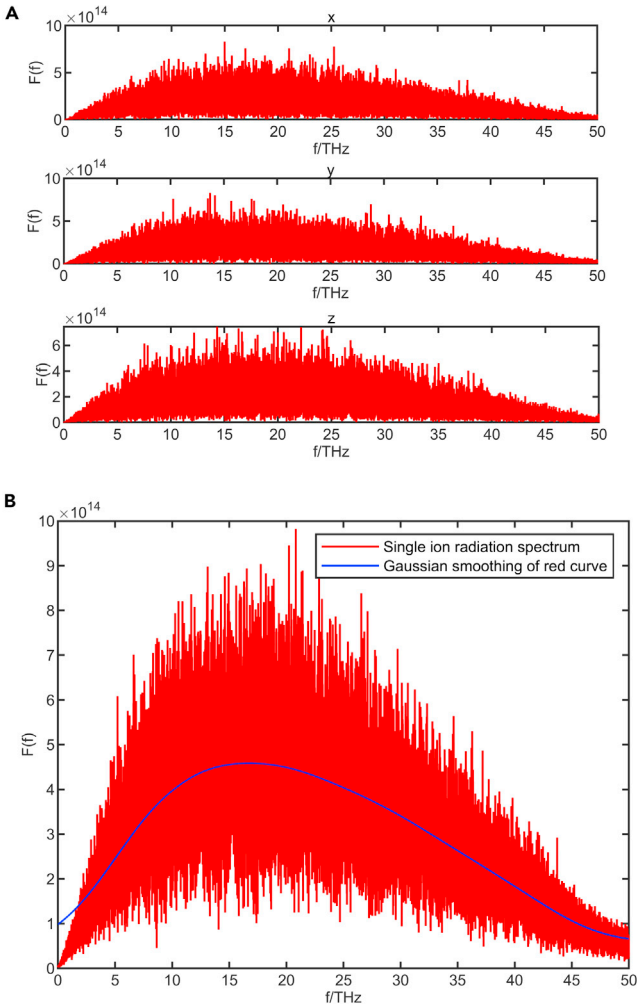


**Figure 8. Radiation spectrum produced by $Ca^{2+}$ in the calcium channel**

(A) The radiation spectrum of a $Ca^{2+}$ moving in a channel in the directions of x, y, z.

(B) The total radiation spectrum of a $Ca^{2+}$ moving in the channel. The blue curve is obtained by Gaussian smoothing of the red curve, and the spectrum of $Ca^{2+}$ in the channel is mainly concentrated around 16.9THz.

emission spectrum of the ion when there are two ions in the channel, the spectrum characteristics of which are shown in Figure 9. The results show that the center frequency of the radiation spectrum of the two ions remains the same, but the radiation intensity varies between the ions. Considering the superposition effect of energy, when multiple ions are transported through the membrane, a higher energy will be radiated outward, which can be measured by specific experimental methods.

Because the random thermal motion of ions is correlated with temperature, the effect of temperature on the ion motion is investigated and shown in Figure 10. We selected three temperature values (280K, 310K, and 340K) for this investigation. The dielectric constant of the channel water is assumed to be constant during the simulation. As the temperature increases, the radiation spectrum of $Ca^{2+}$ shifts to higher frequencies. It can be understood that, with the increase in temperature, the thermal movement of ions intensifies, making the radiation spectrum shift to a higher frequency.

## Applied THz electric field effect on single $Ca^{2+}$ transport through the channel

The movement process of ions in calcium channels regulated by THz waves is studied by the BD method. The Schematic diagram is shown in Figure 11. In this section, we discussed the regulation of THz pulses

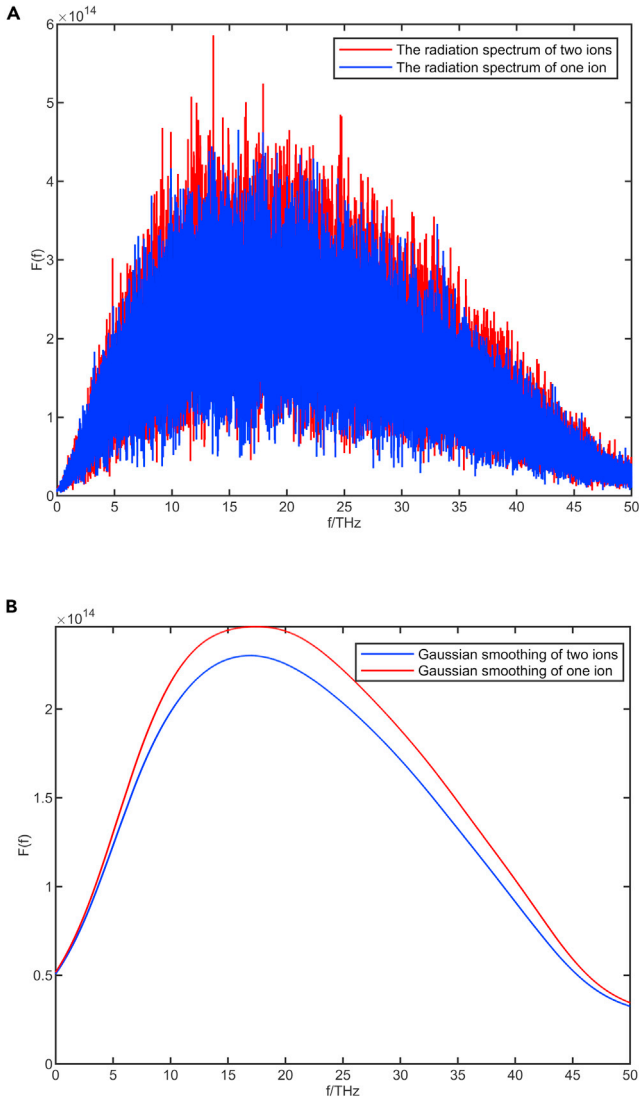


**Figure 9. In the calcium channel, the influence of the number of ions changes on the radiation spectrum of $Ca^{2+}$**

(A) Comparison of the radiation spectra of one $Ca^{2+}$ and two $Ca^{2+}$ in the channel.

(B) The red and blue curves are obtained by Gaussian smoothing of the data in (A).

during the transmembrane process of single ion and multi-ion systems and the changes of the spontaneous emission spectrum of ions under THz irradiation.

Figure 12A shows the effect of unipolar THz pulse trains under different field amplitudes on the transport of single ions through the channel when the frequency is 1 THz. The position of the $Ca^{2+}$ placed in the channel was calculated at each discrete time step of 2 fs for $2\times10^6$ time steps. Figure 12B shows the effect of unipolar THz pulse trains under different frequencies on the transport of a single ion through the channel. The electric field intensity used in this simulation is $-6 \times 10^8$V/m. The results show that the time it takes for $Ca^{2+}$ to cross the channel decreases with the increase of the amplitude. Meanwhile, the time it takes for $Ca^{2+}$ to cross the channel decreases with the increase of the frequency of the THz wave.

In addition, we compare the changes of ion radiation spectrum with or without an external THz field. Here, we focus on the influence of the THz electric field on ion transport across the membrane, while ignoring the influence of the magnetic field. The relevant analysis process can be referred to ref (Bo et al., 2020). We chose the unipolar THz pulse train as the excitation source. The frequency of the applied THz field is

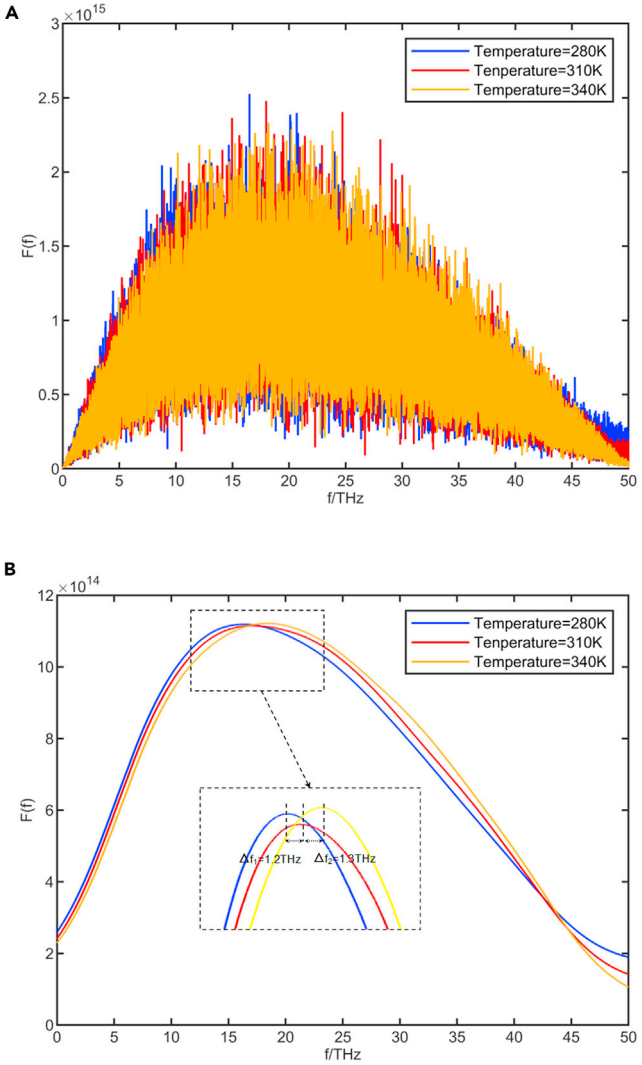


**Figure 10. In the calcium channel, the influence of temperature changes on the radiation spectrum of $Ca^{2+}$**

(A) Spectral characteristics of $Ca^{2+}$ at different temperatures.

(B) The blue, red, and yellow curves are obtained by Gaussian smoothing of the data in (A).

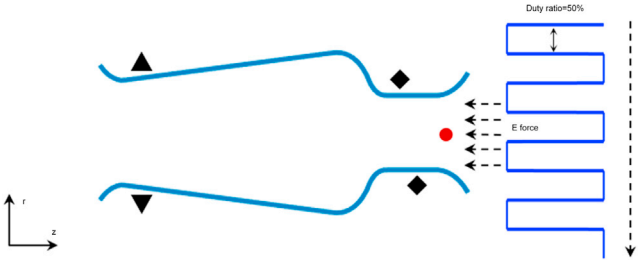


**Figure 11. Schematic diagram of THz wave acting on calcium ion channels**

The THz electric field waveform used in the simulation is a unipolar square wave, and the transmission direction is the r-axis, which is perpendicular to the axial direction of the ion channel; the electric field direction is the z axis, which is parallel to the axial direction of the ion channel.

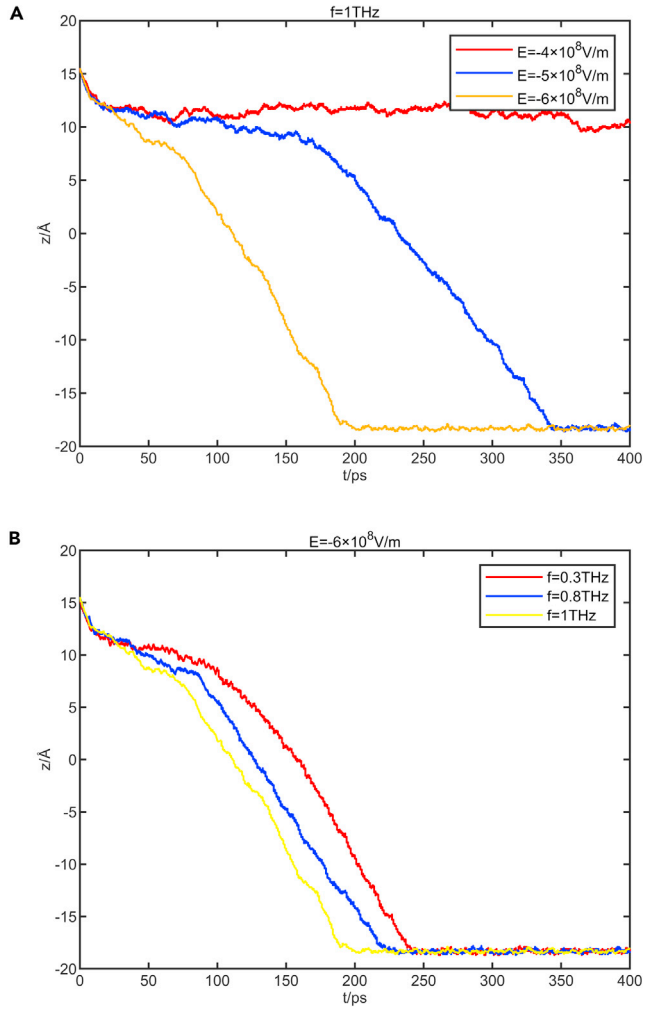


**Figure 12. Trajectories of ions irradiated by unipolar THz waves with different amplitudes and frequencies**

(A) The influence of amplitude changes on $Ca^{2+}$ motion when the frequency is 1THz.

(B) The influence of frequency changes on $Ca^{2+}$ motion when the amplitude is $-6 \times 10^8$V/m.

1THz. The electric field waveforms in the time domain and frequency domain of the THz field are shown in Figure 13A, and the influence of THz waves on the spontaneous emission spectrum of $Ca^{2+}$ is shown in Figure 13B. Under the irradiation of a unipolar THz field, the peak value of the ion's total radiation spectrum is more obvious at low frequency, and the peak position is the same as the peak position of the spectrum of the monopole THz electric field. Meanwhile, the effects of THz electric field irradiation on the radiation spectrum generated by ion oscillation at high frequencies are very weak.

## Applied THz electric field effect on multiple $Ca^{2+}$ transport through the channel

In a practical calcium ion channel, millions of calcium ions pass through the channel every second. And the $Ca^{2+}$ will be subjected to the repulsive forces of multiple ions to accelerate the penetration rate of ions. Figure 14 shows the comparison of the potential energy distribution when there are two ions in the channel with that of a single ion.

Because of the Coulomb repulsion between ions and the effect of the induced charge of the second ion, the energy barrier is reduced. It indicates that the electric field used in the simulation of the multi-ion system is much lower than that of the single-ion system at physiological concentration. To obtain a better statistic, six $Ca^{2+}$ are put on the right side of the channel. Without the external field, $Ca^{2+}$ would be attracted to

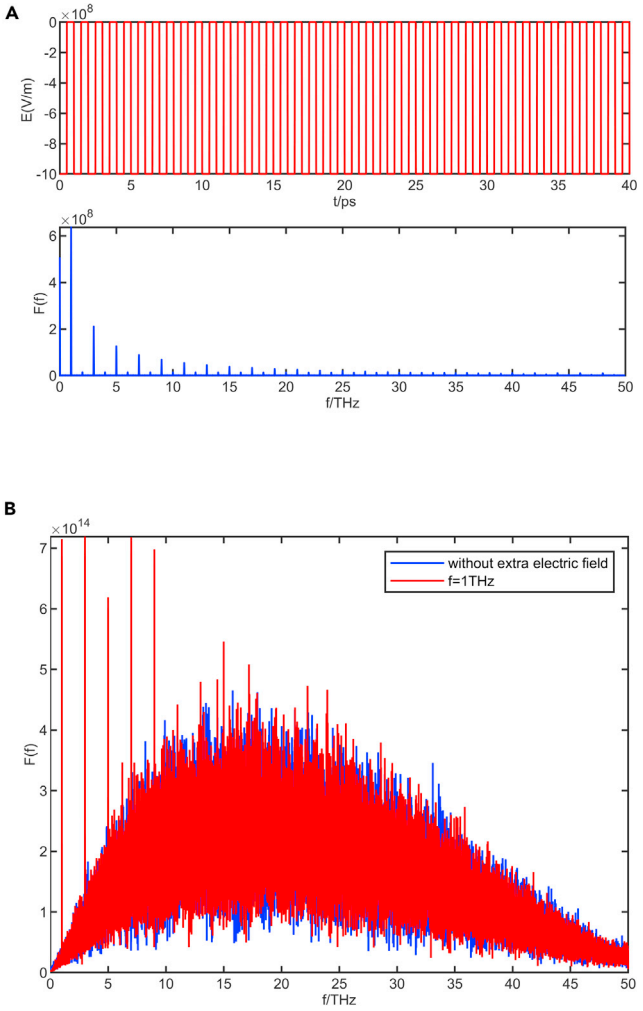


**Figure 13. Effect of THz electric field on the spontaneous emission spectrum of ions**

(A) Time-domain and frequency-domain waveforms of the THz field used in the simulation.

(B) Radiation spectrum of ion motion under THz wave irradiation.

the glutamate groups to move to the vicinity of the channel neck. In this section, we mainly care about the movement of ions from one side of the channel to the other side. Thus, we assume that the movement of ions will not cause significant changes in the concentration of calcium ions on both sides of the membrane within the calculation of nanosecond magnitude. When an ion moves from the right to the left of the channel, a new $Ca^{2+}$ will automatically fill the right side. The amplitude of the applied electric field is $-3 \times 10^8$V/m, the variation of the number of ions across the channel with time in 8 ns is shown in Figure 15. The results show that as the frequency increases, the number of transmembrane ions increases significantly at the same time, which indicated that the high-frequency THz field was more conducive to regulating $Ca^{2+}$ transmembrane penetration.

## Conclusions

In this work, we established a mathematical physical model of the $Ca^{2+}$ channel by the Brownian dynamic method. The time domain and frequency domain characteristics of calcium ion movement in the channel have been analyzed. The results show that the $Ca^{2+}$ transmembrane transport is a rapid signal change process on a short timescale, and its spontaneous radiation spectrum is mainly concentrated in the THz range. Meanwhile, the changes in temperature and the number of ions in the channel were proved to have significant effects on the spectral characteristics, as the frequency increases, the radiation spectrum of calcium

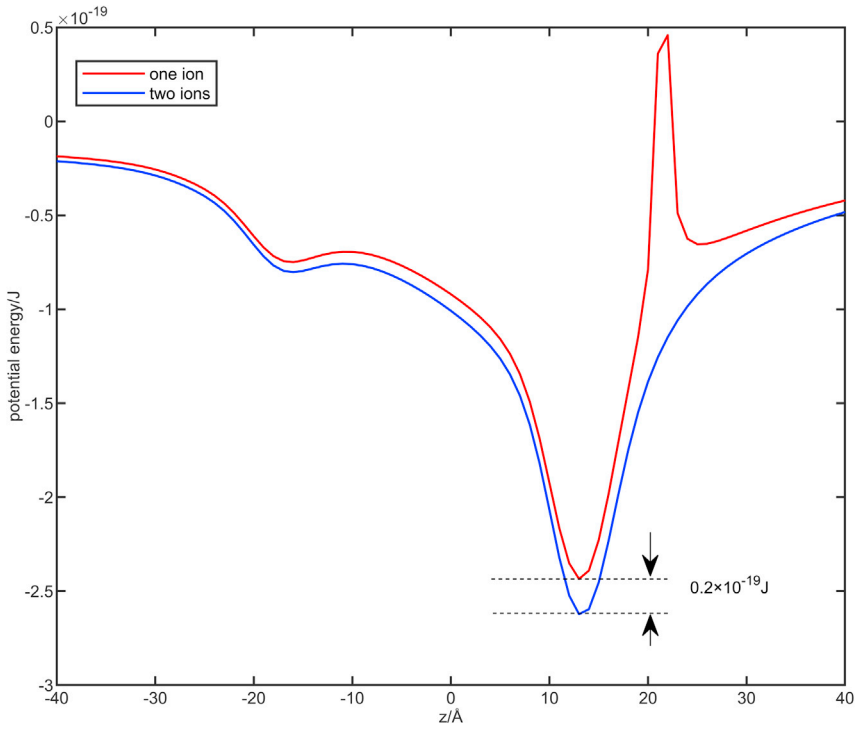


**Figure 14. The potential energy on the axis of the channel**

The blue line represents the potential energy curve of a single $Ca^{2+}$. The red line represents the potential energy curve of one calcium ion under the influence of another ion in the channel neck. The coordinate of the calcium ion in the channel neck is (0, 0, 21.5Å).

ions shifted toward higher frequencies. In addition, under the external THz field irradiation, the oscillation spectrum of the irritated $Ca^{2+}$ is significantly enhanced, which is expected to be applied in future nondestructive testing. It was also found from the simulation results that the transport process of $Ca^{2+}$ across the ion channel is related to the frequency and amplitude of the THz wave. Under a certain amplitude, the ion permeability gradually increases as the frequency of the THz field increases; under a certain frequency, the ion permeability also increases as the amplitude increases. The finding in this paper provides a theoretical basis for the future treatment of THz waves in the neurological field.

## Limitations of the study

The study is theoretical. The interaction between THz waves with ions in channels of nerve cells needs further experimental investigation.

## STAR★METHODS

Detailed methods are provided in the online version of this paper and include the following:

- KEY RESOURCES TABLE
- RESOURCE AVAILABILITY
  - Lead contact
  - Materials availability
  - Data and code availability
- EXPERIMENTAL MODEL AND SUBJECT DETAILS
- METHOD DETAILS
  - BD calculation method
  - Poisson equation solution
  - Channel potential energy calculation method
- QUANTIFICATION AND STATISTICAL ANALYSIS

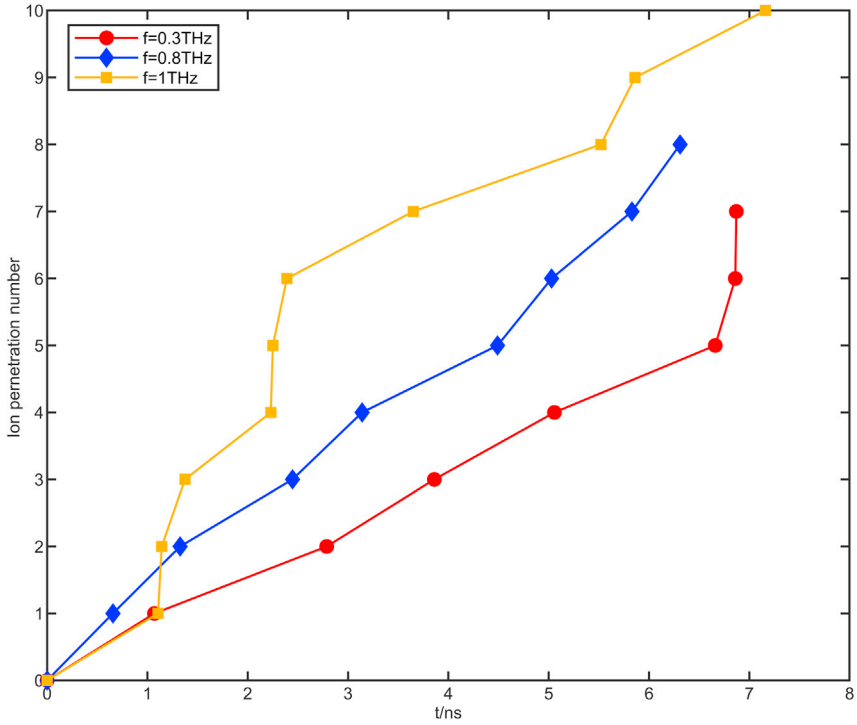


**Figure 15. The variation of ion transmembrane number with time under the control of THz pulses of different frequencies**

The amplitude of the applied electric field is $-3 \times 10^8$V/m. The total calculation time is 8 ns, and the time step is 2fs.

## ACKNOWLEDGMENTS

This work was supported by the National Natural Science Foundation of China (61921002, 61988102).

## AUTHOR CONTRIBUTIONS

Y. G. conceived the project. L. G. and B. W. constructed the physical model of the calcium channel and completed the main theoretical calculation. L. G., K. W., S. W., and Y. G. drafted the manuscript, as well as analyzed and interpreted the data. All authors approved the final version of the manuscript.

## DECLARATION OF INTERESTS

The authors declare no competing interests.

Received: June 30, 2021
Revised: November 15, 2021
Accepted: December 1, 2021
Published: January 21, 2022

## REFERENCES

Bahinski, A., Yatani, A., Mikala, G., Tang, S., and Schwartz, A. (1997). Charged amino acids near the pore entrance influence ion-conduction of a human L-type cardiac calcium channel. Mol. Cell. Biochem. *166*, 125–134. https://doi.org/10.1023/A:1006847632410.

Bo, W., Guo, L., Yang, Y., Ma, J., and Gong, Y. (2020). Numervical study of voltage-gated Ca2+ transport irradiated by terahertz electromagnetic wave. IEEE Access *99*, 1. https://doi.org/10.1109/ACCESS.2020.2964780.

Caterina, M.J., Schumacher, M.A., Tominaga, M., Rosen, T.A., Levine, J.D., and Julius, D. (1997). The capsaicin receptor: a heat-activated ion channel in the pain pathway. Nature *6653*, 816–824. https://doi.org/10.1038/39807.

Chung, S.-H., Allen, T.W., Hoyles, M., and Kuyucak, S. (1999). Permeation of ions across the potassium channel: brownian dynamics studies. Biophys. J. *77*, 2517–2533. https://doi.org/10.1016/S0006-3495(99)77087-6.

Corry, B., Allen, T.W., Kuyucak, S., and Chung, S.H. (2001). Mechanisms of permeation and selectivity in calcium channels. Biophys. J. *80*, 195–214. https://doi.org/10.1016/S0006-3495(01)76007-9.

Ellinor, P.T., Yang, J., Sather, W.A., Zhang, J.F., and Tsien, R.W. (1995). $Ca^{2+}$ channel selectivity at

a single locus for high-affinity Ca2+ interactions. Neuron *15*, 1121–1132. https://doi.org/10.1016/0896-6273(95)90100-0.

Guàrdia, E., and Padró, J.A. (1996). On the influence of the ionic charge on the mean force potential of ion-pairs in water. J. Chem. Phys. *104*, 7219–7222. https://doi.org/10.1063/1.471434.

Guàrdia, E., Rey, R., and Padró, J.A. (1991a). Na+–Na+ and Cl−–Cl− ion pairs in water: mean force potentials by constrained molecular dynamics. J. Chem. Phys. *4*, 2823–2831. https://doi.org/10.1063/1.460934.

Guàrdia, E., Rey, R., and Padró, J.A. (1991b). Potential of mean force by constrained molecular dynamics: a sodium chloride ion-pair in water. Chem. Phys. *155*, 187–195. https://doi.org/10.1016/0301-0104(91)87019-R.

Guàrdia, E., Robinson, A., and Padró, J.A. (1993). Mean force potential for the calcium–chloride ion pair in water. J. Chem. Phys. *99*, 4229–4230. https://doi.org/10.1063/1.466076.

Gunsteren, W.V., and Berendsen, H. (1982). Algorithms for brownian dynamics. Mol. Phys. *45*, 637–647. https://doi.org/10.1080/00268978200100491.

Gunsteren, W., Berendsen, H., and Rullmann, J. (1981). Stochastic dynamics for molecules with constraints. Mol. Phys. *44*, 69–95. https://doi.org/10.1080/00268978100102291.

Guo, L., Bo, W., Wang, K., Wang, S., and Gong, Y. (2021a). Regulation of calcium ion transport by THz wave. https://doi.org/10.5281/zenodo.5720258.

Guo, L., Bo, W., Wang, K., Wang, S., and Gong, Y. (2021b). Calcium Channel Model [Data Set] (Zenodo). https://doi.org/10.5281/zenodo.5728726.

Hoyles, M., Kuyucak, S., and Chung, S.H. (1996). Energy barrier presented to ions by the vestibule of the biological membrane channel. Biophys. J. *70*, 1628–1642. https://doi.org/10.1016/S0006-3495(96)79726-6.

Hoyles, M., Kuyucak, S., and Chung, S.H. (1998). Computer simulation of ion conductance in membrane channels. Phys. Rev. E Stat. Phys. Plasmas Fluids Relat. Interdiscip. Top. *58*, 3654–3661. https://doi.org/10.1103/PhysRevE.58.3654.

Ibsen, S., Tong, A., Schutt, C., Esener, S., and Chalasani, S.H. (2015). Sonogenetics is a non-invasive approach to activating neurons in Caenorhabditis elegans. Nat. Commun. *6*, 8264. https://doi.org/10.1038/ncomms9264.

Jackson, J.D. (1999). Radiation by moving charge. In Classical Electrodynamics, J.D. Jackson, ed. (American Association of Physics Teachers), p. 665. https://doi.org/10.1119/1.19136.

Kato, H.E., Zhang, F., Yizhar, O., Ramakrishnan, C., Nishizawa, T., Hirata, K., Ito, J., Aita, Y., Tsukazaki, T., Hayashi, S., Hegemann, P., et al. (2012). Crystal structure of the channelrhodopsin light-gated cation channel. Nature *482*, 369. https://doi.org/10.1038/nature10870.

Kumar, S., Boone, K., Tuszyński, J., Barclay, P., and Simon, C. (2016). Possible existence of optical communication channels in the brain. Sci. Rep. *1*, 1–13. https://doi.org/10.1038/srep36508.

Li, S.C., Hoyles, M., Kuyucak, S., and Chung, S.H. (1998). Brownian dynamics study of ion transport in the vestibule of membrane channels. Biophys. J. *74*, 37–47. https://doi.org/10.1016/S0006-3495(98)77764-1.

Li, Y., Chang, C., Zhu, Z., Sun, L., and Fan, C. (2021). Terahertz wave enhances permeability of the voltage-gated calcium channel. J. Am. Chem. Soc. *143*, 4311–4318. https://doi.org/10.1021/jacs.0c09401.

Liu, G. (2018). The conjectures on physical mechanism of vertebrate nervous system. Chin. Sci. Bull. *63*, 3864–3865. https://doi.org/10.1360/N972018-01143.

Liu, G., Chang, C., Qiao, Z., Wu, K., Zhu, Z., Cui, G., Peng, W., Tang, Y., Li, J., and Fan, C. (2019). Myelin sheath as a dielectric waveguide for signal propagation in the mid-infrared to terahertz spectral range. Adv. Funct. Mater. *29*, 1807862. https://doi.org/10.1002/adfm.201807862.

McCleskey, E.W., and Almers, W. (1985). The Ca channel in skeletal muscle is a large pore. Proc. Natl. Acad. Sci. U S A *82*, 7149–7153. https://doi.org/10.1073/pnas.82.20.7149.

Miller, L.M., and Dumas, P. (2010). From structure to cellular mechanism with infrared microspectroscopy. Curr. Opin. Struct. Biol. *20*, 649–656. https://doi.org/10.1016/j.sbi.2010.07.007.

Orrenius, S., Zhivotovsky, B., and Nicotera, P. (2003). Regulation of cell death: the calcium-apoptosis link. Nat. Rev. Mol. Cell. Biol. *4*, 552–565. https://doi.org/10.1038/nrm1150.

Ranade, S.S., Syeda, R., and Patapoutian, A. (2015). Mechanically activated ion channels. Neuron *6*, 1162–1179. https://doi.org/10.1016/j.neuron.2015.08.032.

Stillinger, F.H., and Rahman, A. (1974). Improved simulation of liquid water by molecular dynamics. J. Chem. Phys. *60*, 1545–1557. https://doi.org/10.1063/1.1681229.

Tansel, B., Sager, J., Rector, T., Garland, J., Strayer, R.F., Levine, L., Roberts, M., Hummerick, M., and Bauer, J. (2006). Significance of hydrated radius and hydration shells on ionic permeability during nanofiltration in dead end and cross flow modes. Sep. Purif. Technol. *51*, 40–47. https://doi.org/10.1016/j.seppur.2005.12.020.

Wang, K., Yang, L., Wang, S., Guo, L., and Gong, Y. (2020). Transient proton transfer of base pair hydrogen bonds induced by intense terahertz radiation. Phys. Chem. Chem. Phys. *22*, 9316–9321. https://doi.org/10.1039/D0CP01247E.

Wetzel, D.L., and LeVine, S.M. (1999). Imaging molecular chemistry with infrared microscopy. (cover story). Science *285*, 1224. https://doi.org/10.1126/science.285.5431.1224.

Wu, K., Qi, C., Zhu, Z., Wang, C., and Chang, C. (2020). Terahertz wave accelerates DNA unwinding: a molecular dynamics simulation study. J. Phys. Chem. Lett. *17*, 7002–7008. https://doi.org/10.1021/acs.jpclett.0c01850.

Zangari, A., Micheli, D., Galeazzi, R., and Tozzi, A. (2018). Node of Ranvier as an array of bio-nanoantennas for infrared communication in nerve tissue. Sci. Rep. *8*, 539. https://doi.org/10.1038/s41598-017-18866-x.

# STAR★METHODS

## KEY RESOURCES TABLE

| REAGENT or RESOURCE | SOURCE | IDENTIFIER |
|---|---|---|
| Deposited data | | |
| Calcium channel model | This paper | https://doi.org/10.5281/zenodo.5728726 |
| Software and algorithms | | |
| MATLAB | Mathworks | https://www.mathworks.com/ |
| Regulation of calcium ion transport by THz wave algorithm | This paper | https://doi.org/10.5281/zenodo.5720258 |

## RESOURCE AVAILABILITY

### Lead contact

Further information and requests for resources should be directed to the lead contact, Yubin Gong (ybgong@uestc.edu.cn).

### Materials availability

This study did not generate new unique reagents.

### Data and code availability

- The calcium ion channel model and the potential distribution in 3D calcium ion channel data have been deposited at Zenodo (Guo et al., 2021b) and are publicly available as of the date of publication. Accession numbers are listed in the key resources table. The DOI is listed in the key resources table. Any additional data reported in this paper will be shared by the lead contact upon request.
- All original code has been deposited at Zenodo (Guo et al., 2021a) and is publicly available as of the date of publication. DOIs are listed in the key resources table.
- Any additional information required to reanalyze the data reported in this working paper is available from the lead contact upon request (ybgong@uestc.edu.cn).

## EXPERIMENTAL MODEL AND SUBJECT DETAILS

Our study does not use experimental models typical in the life sciences.

## METHOD DETAILS

### BD calculation method

In BD (Gunsteren et al., 1981; Hoyles et al., 1996), the movement of a single ion through the membrane is determined by the Langevin equation of motion,

$$m_i \frac{d\vec{v}_i(t)}{dt} = -m_i\gamma_i\vec{v}_i(t) + \vec{F}_R(t) + \vec{F}_E(t) + \vec{F}_S(t) \quad \text{(Equation 2)}$$

where $m_i$ is the ion's mass; $\vec{v_i}(t)$ is the vector velocity of the ion at time $t$; $\gamma_i$ is the damping coefficient which reflects the average frictional force under the action of water molecules around the ion; $\vec{F_S}$ is the random forces; $\vec{F_E}$ is the electric field force generated by ions and the applied THz field; $\vec{F_R}$ represents the short-range forces, including collisions between ions and the repelling force of the channel boundary on the ion, which is used to maintain the stability of the system to avoid ions' overlap and crossing of the water-protein interface.

In this simulation, we applied a rigid boundary on the inner surface of the channel to prevent ions from crossing the boundary (Corry et al., 2001). Therefore, the ion moving toward the channel's inner surface will be repelled back. The short-range force between $Ca^{2+}$ and the boundary can be expressed as (Guàrdia et al., 1991a, b),

$$\overrightarrow{F}_{Rb}(r) = F_0 \frac{(R_i + R_w)^{10}}{(R_b(z) + R_w - r)^{10}} \quad \text{(Equation 3)}$$

where $F_0$ is the force field parameter, $R_i$ is the radius of ion, $R_w$ is the radius of boundary wall atoms, r is the distance between the ion and the central axis, and $R_b$ is the distance between the channel wall and the central axis in the corresponding z coordinate.

For the ions moving in the channel, the forces between multiple ions are mainly described by the Coulomb force and the short-range force between ions. The short-range force (Guàrdia et al., 1991a, b) between two ions with separation r can be expressed as,

$$\overrightarrow{F}_{Ri}(r) = -C_0 \left[ \frac{-9(R_1 + R_2 + C_1)^9}{r^{10}} + \frac{1}{C_3} e^{(R_1 + R_2 + C_2 - r)/C_3} \cos[2\pi(R_1 + R_2 + C_2 - r)/c_w] - (2\pi/c_w) e^{(R_1 + R_2 + C_2 - r)/C_3} \sin[2\pi(R_1 + R_2 + C_2 - r)/c_w] \right] \quad \text{(Equation 4)}$$

where $R_1$and $R_2$ are the radii of the two ions. The meanings and values of coefficients $C_0$, $C_1$, $C_2$, $C_3$, $c_w$ are listed in Table 1, which are provided from Ref. (Corry et al., 2001; Guàrdia and Padró, 1996; Guàrdia et al., 1993).

the Langevin Equation (2) can multiply the integrating factor $e^{\gamma_i t}$ and be integrated from an initial time $t_n$ to $t_{n+1}$ ,

$$m_i \int_{t_n}^{t_{n+1}} \frac{dv_i}{dt} e^{\gamma_i t} dt = \int_{t_n}^{t_{n+1}} \overrightarrow{F}_S e^{\gamma_i t} dt + q_i \int_{t_n}^{t_{n+1}} \left( \overrightarrow{F}_E + \overrightarrow{F}_R \right) e^{\gamma_i t} dt - \int_{t_n}^{t_{n+1}} \gamma_i v_i e^{\gamma_i t} dt \quad \text{(Equation 5)}$$

In addition to random forces, the forces exerted on the ion are denoted by $\overrightarrow{F}$. Then, we can get an expression for the ion velocity

$$v_i(t_{n+1}) = v_i(t_n) e^{-\gamma_i(t_{n+1} - t_n)} + \frac{e^{-\gamma_i t}}{m} \int_{t_n}^{t_{n+1}} \overrightarrow{F}_S e^{\gamma_i t'} dt' + \frac{1}{m\gamma} e^{-\gamma_i t} \int_{t_n}^{t_{n+1}} \overrightarrow{F} d e^{\gamma_i t'} \quad \text{(Equation 6)}$$

Taylor expansion of $\overrightarrow{F}$ at $t_n$,

$$\overrightarrow{F}(t_{n+1}) = \overrightarrow{F}(t_n) + \overrightarrow{F}'(t_n)(t_{n+1} - t_n) + \ldots \quad \text{(Equation 7)}$$

Substitute Equation (7) into (6), and then we can get,

$$v_i(t_{n+1}) = v_i(t_n) e^{-\gamma_i(t_{n+1} - t_n)} + \frac{\overrightarrow{F}(t_n)}{m\gamma_i} \left(1 - e^{-\gamma_i(t_{n+1} - t_n)}\right) + \frac{\overrightarrow{F}'(t_n)}{m{\gamma_i}^2} \left[\gamma_i(t_{n+1} - t_n) - 1 + e^{-\gamma_i(t_{n+1} - t_n)}\right] + \frac{e^{-\gamma_i t_{n+1}}}{m} \int_{t_n}^{t_{n+1}} \overrightarrow{F}_S e^{\gamma_i t'} dt' \quad \text{(Equation 8)}$$

By integrating (8) from an initial time $t_n$ to $t_{n+1}$, the position of the ion at the next moment can be obtained. Here, the result of integrating the last term of Equation (8) is expressed in terms of a defined $X_n$ variable,

$$\overrightarrow{s}_i(t_{n+1}) = \overrightarrow{s}_i(t_n) + \frac{v_i(t_n)}{\gamma_i}(1 - e^{-\tau}) + \frac{\overrightarrow{F}(t_n)}{m{\gamma_i}^2}(\tau - 1 + e^{-\tau}) + \frac{\overrightarrow{F}'(t_n)}{m{\gamma_i}^3}\left(\frac{\tau^2}{2} - \tau + 1 - e^{-\tau}\right) + X_n(\Delta t) \quad \text{(Equation 9)}$$

Where, $\tau$=$\gamma(t_{n+1}$-$t_n)$. The expression without velocity term can be obtained from Equations (8) and (9),

$$\overrightarrow{s}_i(t_{n+1}) = \overrightarrow{s}_i(t_n)(1 + e^{-\tau}) - \overrightarrow{s}_i(t_{n-1})e^{-\tau} + \frac{\overrightarrow{F}(t_n)}{m{\gamma_i}^2}\tau(1 - e^{-\tau}) + \frac{\overrightarrow{F}'(t_n)}{m{\gamma_i}^3}\left(\frac{\tau^2}{2}(1 + e^{-\tau}) - \tau(1 - e^{-\tau})\right) + X_n(\Delta t) - X_n(-\Delta t)e^{-\tau} \quad \text{(Equation 10)}$$

$$\overrightarrow{v}_i\left(t_n\right) = \frac{2\gamma_i}{\sinh\tau}\left[\overrightarrow{s}_i\left(t_{n+1}\right) - \overrightarrow{s}_i\left(t_{n-1}\right) + 2\left(\frac{\overrightarrow{F}\left(t_n\right)}{m{\gamma_i}^2} - \frac{\overrightarrow{F}'\left(t_n\right)}{m{\gamma_i}^3}\right) \cdot (\sin\tau - \tau) - X_n(\Delta t) + X_n(-\Delta t)\right] \quad \text{(Equation 11)}$$

$X_n(\Delta t)$ is the random variable used in the BD algorithm, which obeys Gaussian distribution with a mean value of 0 and a variance of $2K_BT\Delta t/m_i\gamma_i=2D_i\Delta t$. One can refer to Ref. (Gunsteren and Berendsen, 1982) for details. Equations (10) and (11) are the displacement and velocity equations of ions, which are used to calculate the displacement and velocity of $Ca^{2+}$ in the channel.

The total electric field force can be written as the following form,

$$\vec{F}_E = \vec{F}_i + \sum_{i\neq j}^{n} \vec{F}_{j,i} + \vec{F}_{THz} \quad \text{(Equation 12)}$$

where $\vec{F}_i$ is the force of induced charge generated by the induction of ions at the water-protein interface; $\vec{F}_{j,i}$ is the force on the ion $i$ generated by other ions in the channel; $\vec{F}_{THz}$ is the electric field force generated by the applied THz electric field. The electric field waveform used in the simulation in this paper is a unipolar square waveform. Here, since the motion velocities of ions are much smaller than the light speed, the effect of the magnetic field on the motion of ions is not considered (Bo et al., 2020). The values of the parameters are listed in Table 1.

## Poisson equation solution

The total electric field at the ion position is determined by the solution of the Poisson equation,

$$\nabla[\varepsilon_r\nabla\varphi(r)] = -(\rho_0(r) + \rho_d(r))/\varepsilon_0 \quad \text{(Equation 13)}$$

where $\rho_0$ represents the charge density of the ion, $\rho_d$ represents the charge density of the negatively charged residues at the channel boundary and the channel dipole. $\varepsilon_0$represents the vacuum dielectric constant, which is $8.85\times10^{-12}$. $\varepsilon_1$ and $\varepsilon_2$ represent the permittivity of water in the channel and channel protein, and the values are 60 and 2, respectively. The total potential in the channel can be expressed as follows,

$$\varphi = \sum_i \varphi_i + \varphi_d + \varphi_e \quad \text{(Equation 14)}$$

where $\varphi_i$ is the self-potential due to the ion and the induced charge on the channel wall, $\varphi_d$ is the external potential due to the negatively charged groups, and the dipole on the channel wall, $\varphi_e$ is the external potential due to the applied field.

To get the potential distribution of the channel, we replace this model with an equivalent model having a dielectric constant $\varepsilon_1$ that produces the same electrical potential throughout space. Furthermore, the discontinuity boundary between channel water and channel protein under the electric field is replaced by polarization charge density $\rho_1$. Thus, the potential of Equation (13) can be expressed by,

$$\varphi(r) = \frac{1}{4\pi\varepsilon_1\varepsilon_0}\left[\sum_{i=1}^{n}\frac{q_i\delta_i(r)}{R_i(r)} + \int_S \frac{\rho_1 dS}{R_1(r')}\right] \quad \text{(Equation 15)}$$

$$\rho_1 = 2\varepsilon_0\frac{\varepsilon_2-\varepsilon_1}{\varepsilon_2+\varepsilon_1}\cdot\vec{E}\cdot\vec{n} \quad \text{(Equation 16)}$$

By iteratively solving Equations (15) and (16), we can get the potential distribution of the ion channel. Here, $\vec{n}$ is the normal direction of the boundary. The criterion for convergence is that when the ratio of the polarization charge density $\rho_1$ difference between the two iterations to the maximum charge density is less than 0.001%, we consider the result to be convergent.

## Channel potential energy calculation method

The energy difference caused by neglecting the change of the dielectric constant of water is approximately given by the Born energy,

$$E_B = \frac{{q_{Ca}}^2}{8\pi\varepsilon_0 R_B}\left(\frac{1}{\varepsilon_1}-\frac{1}{\varepsilon_v}\right) \quad \text{(Equation 17)}$$

Where $R_B$ is the ionic hydration radius, $\varepsilon_v$ is the dielectric constant of free water, the value is 78. $\varepsilon_1$ is the dielectric constant of water in the channel, and the value is 60. Here, a smooth switching function (Chung et al., 1999) is used to avoid complications arising from sharp potential energy changes in BD simulations, which can implement this potential barrier,

$$U_B(R) = (E_B/16)\left(3R^5 - 10R^3 + 15R\right) + E_B/2$$

$$R = \begin{cases} \dfrac{z - 1.8 \times 10^{-9}}{0.2 \times 10^{-9}}, 1.6 \times 10^{-9} \leq z \leq 2.0 \times 10^{-9} \\ \dfrac{z + 2.2 \times 10^{-9}}{0.2 \times 10^{-9}}, -2.4 \times 10^{-9} \leq z \leq -2 \times 10^{-9} \end{cases} \quad \text{(Equation 18)}$$

The potential energy (Chung et al., 1999) can be calculated by:

$$U_{total} = \sum_i \frac{q}{2}[2(\varphi_d + \varphi_e) + \varphi_i] + U_B \quad \text{(Equation 19)}$$

## QUANTIFICATION AND STATISTICAL ANALYSIS

The BD program used in the simulations is written in MATLAB software and executed in the server with the Intel(R) Core(TM) i7-8700k CPU and 32GB memory. The algorithms have been deposited at Zenodo (Guo et al., 2021a, 2021b). The main calculation process includes two steps. First, the three-dimensional space is discretized into 11 × 11×44 points. The potential distributions of the channel for ions at different positions are pre-calculated which are stored in the 4-D data table, which has been deposited at Zenodo (Guo et al., 2021a, 2021b). The CPU time of a server for completing the whole calculation of the three-dimensional potential is about 6 h. Then, the Langevin equation of motion is solved and the positions and velocities of the ions at different times are obtained. By referring to the data table established in the first step, the electric field forces of ions at different positions can be obtained. The time step used in the dynamics simulation is 2 fs, and the temperature is 310 K. With one ion in the reservoirs, the CPU time of a server for completing a single simulation period of 400ps ($2\times10^6$ time steps in 2 fs) is about 20 min.